




Electronic stopping power in titanium for proton and helium ions from first-principle calculationsChang-Kai Li ¹, Jian-ming Xue,^{1,*} Xiao-ping OuYang ^{1,2} and Feng-Shou Zhang ^{2,3,4}¹*State Key Laboratory of Nuclear Physics and Technology, School of Physics, Peking University, Beijing 100871, China*²*The Key Laboratory of Beam Technology and Material Modification of Ministry of Education, College of Nuclear Science and Technology, Beijing Normal University Beijing 100875, China*³*Beijing Radiation Center, Beijing 100875, China*⁴*Center of Theoretical Nuclear Physics, National Laboratory of Heavy Ion Accelerator of Lanzhou, Lanzhou 730000, China*

(Received 15 November 2022; accepted 10 April 2023; published 20 April 2023)

The energy loss rate from energetic proton and helium ions to electrons of a transition metal titanium (Ti) is studied using real-time time-dependent density functional theory. Nonequilibrium simulations with and without semicore electrons explicitly included in describing the electronic structure of target atoms are performed to understand their involvement in the dissipation mechanism. It is found that the low-lying $3s$ and $3p$ semicore excitations play significant roles in determining the profile of the stopping curve around and above the stopping maximum. Additionally, we investigate the effect of impact geometry on electronic stopping. An important conclusion is that although off-channeling geometry, which makes possible the strong interaction with tightly bound electrons, indeed improves the amplitude of the stopping curve, especially for the regime around the stopping maximum, it does not shift the position of the stopping maximum. Our results about the relation between effective charge and electronic stopping are in qualitative agreement with the linear response theory.

DOI: [10.1103/PhysRevA.107.042813](https://doi.org/10.1103/PhysRevA.107.042813)**I. INTRODUCTION**

Slowing down of swift ions in matter has fueled extensive efforts ever since the early days of atomic physics [1–3]. The mechanism involved is a fundamental problem of many modern technologies such as nuclear fission and fusion reactors [4,5], outer space exploration [6], ion therapy [7,8], biomedical imaging [9], ion beam writing [10], and ion implantation [11]. During the ion-matter interaction, the kinetic ion energy is gradually deposited into the host ionic and electronic degree of freedom. When the charged particle is fast enough (typically greater than the host Fermi velocity v_F) [12], the kinetic ion energy is predominantly lost electronically due to the extremely short interaction time and significant difference in inertia between the nucleus and electron. The dissipative force thus generated is formally referred to as the electronic stopping power S_e , which is typically denoted as the rate of energy transfer from the charged particle to electrons in matter per unit ion path.

Historically, numerous analytical models have been developed to determine the electronic stopping. Rutherford [1], Thomson [13], and Darwin [14] put forward energy transfer formulas based on classical Coulomb scattering. Bohr [2] and Bethe [3] derived stopping power formulas using classical and quantum mechanical perturbation theory, respectively. Subsequently, Fermi and Teller [15] proposed electron gas models, and Lindhard [16] developed the dielectric formalism treatment based on linear response theory. These approaches predict electronic stopping with varied degrees of success

depending on the impact velocity and the nature of the ion-target combination. More detailed introduction about the analytical methods can be found in the review by Race *et al.* [17].

Over the past few decades, the advances in modern electronic structural methods and high-performance computing have opened the door to obtaining key parameters such as electron density and screened potential in analytical models directly from first-principles theories in a self-consistent way [18–21]. Such a parameter-free method is expected to go tremendously beyond analytical models, as it provides direct access to the coupling of electronic and ionic degrees of freedom, making it possible to study the nature of the electronic excitations during the ion-matter collision. Especially, the recent development of time-dependent density-functional theory (TDDFT) captures the ever-changing characteristics of electron density and screened potential during ion-target interaction. [22–27]. Nevertheless, modern nonequilibrium TDDFT explicitly takes into account the effects of inhomogeneity in electron density arising from the underlying lattice structure [24,28–30], band structure [31], and band gap [22,25,26], which are important to the electronic stopping but difficult to incorporate in analytical models, and also the first-principles theories based on the free electron gas.

In the early years when fully first-principles nonequilibrium TDDFT calculations of electronic stopping were first developed, great interest was devoted to investigate electronic stopping of slow ions (with velocity below Bohr velocity) [22,26,32–35], the induced electronic excitations of which predominantly arise from the weakly bound valence shell. In recent years, nonequilibrium TDDFT also shows great potential to predict electronic stopping even for the higher

*Corresponding author: jmxue@pku.edu.cn

velocity regime around and above the stopping maximum [27,36–42], with the inclusion of the low-lying inner-shell configurations. Up to now, a variety of research works have been devoted to exploring the contribution of inner-shell electrons. Ojanperä *et al.* [41] reported that the inner-shell electrons of both the projectile and the target contribute to the electronic stopping. Schleife *et al.* [40] pointed out the necessity of taking inner-shell electrons and off-channeling geometry into account to accurately predict the electronic stopping. Ullah *et al.* [27] studied the importance of low-lying level state electrons of both the projectile and target in self-irradiated Ni. In the research of protons in water, Yao *et al.* [38] found that the *K*-shell core-electron excitation is important to the electronic stopping for the velocity regime above stopping maximum. Lee *et al.* [39] reported that inner-shell electrons significantly affect electronic stopping and also have an unexpected influence on the charge state of the projectile. Li *et al.* [43] quantitatively investigated the effect of electronic screening from projectile inner-shell configuration on the electronic stopping.

In this work, TDDFT coupling Ehrenfest molecular dynamics (EMD) [44], we mainly investigate a sophisticated way [40] to accurately predict the electronic stopping over a wide range of velocities. Specifically, the effect of inner-shell excitation on the energy loss rate of low-*Z* proton and helium ions in titanium (Ti) and the mechanism involved is studied in detail. Additionally, we also investigate the difference introduced by channeling and off-channeling impact geometries. In particular, such bi-ion research also facilitates addressing the relation between projectile charge states and the electronic stopping power. The choice of Ti as the target is due to the broad interest in this kind of transition metal and its alloy, and also there are plenty of experimental data available for light ions in Ti.

This article is outlined as follows. In Sec. II, we briefly introduce the theoretical framework and the computational details. Results are presented and discussed in Sec. III, where we concentrate on the following two parts: we first discuss in detail the effect of inner-shell excitation and impact geometry on the electronic stopping in Sec. III A, then in Sec. III B we mainly address the charge state dependence of the electronic stopping. Conclusions are drawn in Sec. IV.

II. MODEL AND METHODS

During the course of the simulation, the energy transferred to the host electronic system from irradiating ions is monitored. For simplicity, and since the S_e is a velocity-resolved quantity, the irradiating ion is constrained to move at a given velocity, thus the total energy of the system is not conserved. Instead of the direct kinetic energy loss of the projectile, the excess in total system energy is used as energy transfer in determining the electronic stopping. First, a ground-state density-functional theory (DFT) calculation is performed to acquire the converged static state of the projectile and host Ti atoms, then the neutral (or screened) irradiating ion is set to move. The target Ti nuclei are frozen in the equilibrium positions, considering their velocity and movement are expected to undergo only a marginal change during the instantaneous interaction [45]. Such practice is also to ensure that all the

perturbations induced by the projectile are limited to the level of electronic degrees of freedom, avoiding the influence of nuclear energy loss on the calculation of electronic stopping.

As the irradiating ion moves, the time-dependent Kohn-Sham (TD-KS) equation describes the evolution of the electron density and energy of the system, due to the dynamics of effective single-particle states under the external potential generated by the projectile and host nuclei. These states evolve in time with a self-consistent Hamiltonian that is a function of electron density $n(\vec{r}, t)$,

$$i\hbar \frac{\partial \varphi_i(\vec{r}, t)}{\partial t} = \left[-\frac{\hbar^2 \nabla^2}{2m} - V_{KS}(n, \{\vec{R}\}) \right] \varphi_i(\vec{r}, t), \quad (1)$$

with

$$n(\vec{r}, t) = \sum_{i=1}^{occ} |\varphi_i(\vec{r}, t)|^2, \quad (2)$$

where $\{\vec{R}\}$ denotes the instantaneous position set of all nuclei. V_{KS} describes the electron-nucleus potential, Hartree potential, and time-dependent exchange-correlation potential. In the present work adiabatic local-density approximation (ALDA) with Perdew–Wang analytic parametrization [46] is employed as the exchange-correlation, and any memory effects [47] of V_{xc} are neglected. Nazarov *et al.* [48] have shown that the error introduced by the adiabatic approximation is negligibly small for low-*Z* ions such as proton and helium ions.

All simulations in this work are carried out using the OCTOPUS *ab initio* real-space code [49,50]. There is no basis set in such code; the external potential, electron density, and KS orbitals are discretized in a set of mesh grid points, and the spacing of the mesh grid corresponds to the energy cutoff in the plane wave basis. The finer the mesh, the larger cutoff energy corresponded. In the present work, a uniform spacing of 0.18 Å along the three spatial coordinates is employed, which corresponds to an energy cutoff of about 1160.6 eV in the plane-wave basis. A small time step of 0.001 fs is adopted to ensure the stability of the time-dependent computations. The convergence of time steps and grid spacings has been tested, and simulations with smaller time steps and grid spacings give essentially the same results (see Sec. A of Supplemental Material [51]). To investigate the effect of inner-shell electron excitation on S_e , two pseudopotentials, namely, Ti4([core]¹⁸3d²4s²) and Ti12([core]¹⁰3s²3p⁶3d²4s²) with four and 12 electrons explicitly included are employed. The electrons frozen in the ionic core cannot polarize or take part in any dynamical process. All the atoms, including the projectile in the present work, are represented by Gaussian-type scalar-relativistic nonlocal pseudopotentials [52], and are factorized in the Kleinman-Bylander form [53].

Periodic boundary conditions are employed throughout this study, and the Ewald method [54,55] is used to sum the long-range interactions between ions in periodic images. The lattice structure employed in this work is three-dimensional (3D) hexagonal with lattice parameters $a = b = 2.95$ Å, $c = 4.68$ Å, $\alpha = \beta = 90^\circ$, $\gamma = 120^\circ$. The convergence of supercell size has been tested (see Sec. B of Supplemental Material [51]), a $4 \times 4 \times 3$ supercell size comprising 96 host atoms and one in-

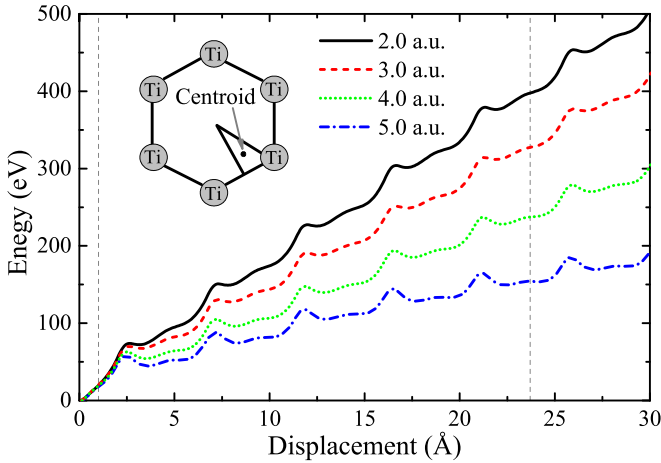


FIG. 1. Increase of system total energy for channeling protons as a function of projectile displacement along the centroid trajectory in the $\langle 100 \rangle$ channel for a projectile with different velocities. The electronic stopping is extracted by linear fitting of the region between the gray lines. The inset shows the sketch of the centroid trajectory.

terstitial projectile atom is chosen so as to reduce the finite size effects while maintaining controllable computational demands. Only one single k point (Γ) is used to integrate the Brillouin zone.

The TDDFT calculations on the electronic system with the moving proton are performed in channeling and off-channeling geometries, respectively. For the channeling case, the “centroid trajectory” suggested in Refs. [37,41,56] is used to represent a classical ensemble average of projectile trajectories. In the off-channeling case, the projectile takes random trajectory directions through the host crystal, yielding occasionally stronger interaction between the projectile and the tightly bound electrons of the host atoms. Instead of converging a classical ensemble average of projectile trajectories, for which it is difficult to determine the weight of each trajectory, one single long simulation as suggested by Schleife *et al.* [40], which circumvents the above-mentioned problem and would explore a wide range of impact parameters and therefore densities, is adopted. In fact, a so-called “random direction” [0.543,0.313,0.779] (given normalized here) which is incommensurate with main crystal directions is used in the present work. We have compared the S_e with results along another direction [0.397,0.229,0.889], and the discrepancies are within 1.6% (see Sec. C of Supplemental Material [51]).

The evolutions of the increase in system total energy with displacement of the projectile for the channeling and off-channeling cases are shown in Figs. 1 and 2, respectively. The key parameter S_e is extracted by linear fitting of the increase in system energy. A kink with a spatial extent of about 1 Å, depending on the impact velocity, in the beginning of the simulation produced by the initial sudden motion of the projectile is abandoned. To avoid the influence of wake potential induced by reentering the simulation cell along the same trajectory, the channeling S_e data are extracted by linear fitting of the increase in system energy within the first two supercells about 23 Å in thickness.

Since the projectile does not reenter the simulation cell on the same path each time for the off-channeling geome-

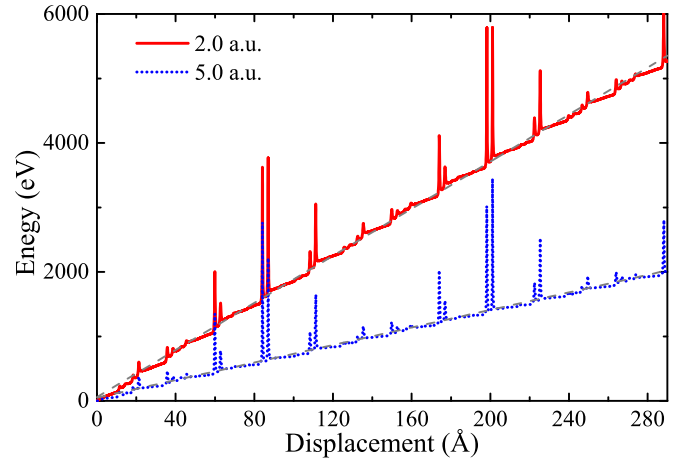


FIG. 2. Increase of system total energy for off-channeling protons with velocity $v = 2.0$ and 5.0 a.u. as a function of projectile displacement. The gray dashed lines show the corresponding slopes of linear fits.

try, reentering does not influence the results as much as in the channeling geometry. The calculated S_e data for the off-channeling case are extracted by linear fitting of the increase in system energy over a long trajectory about 290 Å. The peaks in Fig. 2 represent the close encounter with host nuclei, and the amplitudes reflect the closeness between the projectile and host nuclei. As can be seen, in the off-channeling geometry, much more impact parameters are explored compared to that of channeling geometry, which ensures the “freedom” of the ion trajectory to a large extent.

III. RESULTS AND DISCUSSION

A. Electronic stopping of proton and helium ions

We present in Fig. 3 the simulated S_e results for the motion of proton with velocity of 0.1–6.0 a.u. along the channeling

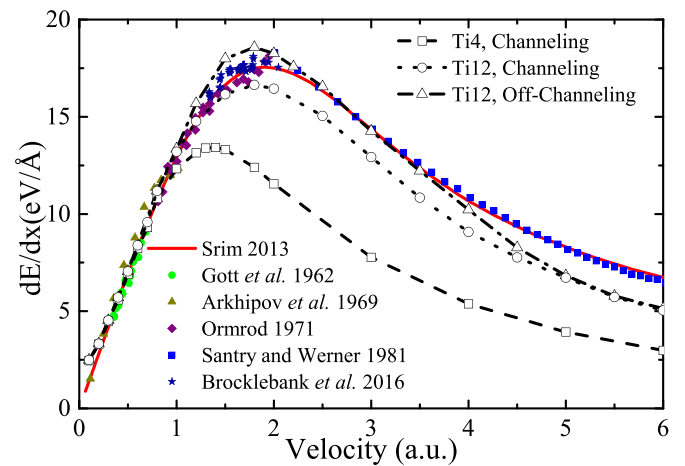


FIG. 3. Simulated electronic stopping power for channeling proton in Ti4 and Ti12 (black open squares and circles) and off-channeling protons in Ti12 (black open up triangle) as a function of velocity, together with the SRIM-2013 predictions (red solid line), experimental data (solid symbols) by Gott [57], Arkhipov [58], Ormrod [59], Santry [60], and Brocklebank [61].

and the off-channeling trajectories. Also shown are the experimental data by Gott [57], Arkhipov [58], Ormrod [59], Santry [60], and Brocklebank [61]. It can be seen that for the channeling geometry, the calculated S_e of protons in Ti4 saturates early at about $v = 1.3$ a.u. and the amplitude of maximum value underestimates about 23% of the experimental data. Such a situation is improved by including the 3s and 3p configurations. For proton interacts with Ti12 under channeling geometry, the agreement between calculated results and experimental data nearly extends up to the stopping maximum, reconfirming the validity of the centroid channeling geometry in the velocity regime below the stopping maximum [43]. However, beyond the stopping maximum, the calculated results for proton channeling Ti12 also underestimate the experimental data (the simulated result is about 17% lower than experimental data at $v = 5.0$ a.u.). For the off-channeling geometry, the calculated electronic stopping of Ti12 for protons at the velocity regime around the stopping maximum is obviously improved, and the agreement with experimental data is excellent up to about $v = 3.5$ a.u., while for the higher velocity regime, the calculated results also underestimate the experimental data (the underestimate is about 15% at $v = 5.0$ a.u.).

First, to investigate the source of the significant difference between S_e for protons in Ti4 and Ti12 around and above the stopping maximum, the electronic excitations in the target are examined. The time-dependent occupation of electronic states is obtained by projecting all time-dependent Kohn-Sham wave functions $\sum_n \psi_n(t)$ onto the ground-state Kohn-Sham orbitals φ_i as [32,62]

$$C_{\text{occ}}(\varepsilon_i) = \sum_n |\langle \varphi_i | \psi_n(t) \rangle|^2, \quad (3)$$

where ε_i is the eigenvalue of φ_i . The total number of excited electrons can be obtained as

$$N = \sum_i^{\varepsilon_i < E_F} [O_{\text{occ}}(\varepsilon_i) - C_{\text{occ}}(\varepsilon_i)] \delta(\varepsilon - \varepsilon_i), \quad (4)$$

where $O_{\text{occ}}(\varepsilon_i)$ is the occupation of the ground-state Kohn-Sham orbitals φ_i .

Under channeling condition, the velocity-resolved number of electrons excited from valence 3d and 4s shells and also that from low-lying 3s and 3p shells are calculated, and it is the instantaneous value at the end of projectile ion path with length 23.7 Å. The results are presented in Fig. 4, and it can be seen that although the valence 3d and 4s shell excitations are dominant, the low-lying 3s and 3p shell excitations are also pronounced. Particularly, the energy dissipated is much higher for the low-lying 3s and 3p shell excitations than that of valence excitation, which promises their significant role in determining the electronic stopping. The position of maximums for the inner 3s and 3p shell excitations and electronic stopping for protons in Ti12 are coincident, indicating that neglected 3s and 3p shell excitations are responsible for the underestimation of S_e for protons in Ti4.

As to the underestimation of S_e for velocities above 3.5 a.u. for protons in Ti12 under both channeling and off-channeling geometries, according to the report by Yao *et al.* [38], the 1s level excitation of oxygen atoms with a binding energy

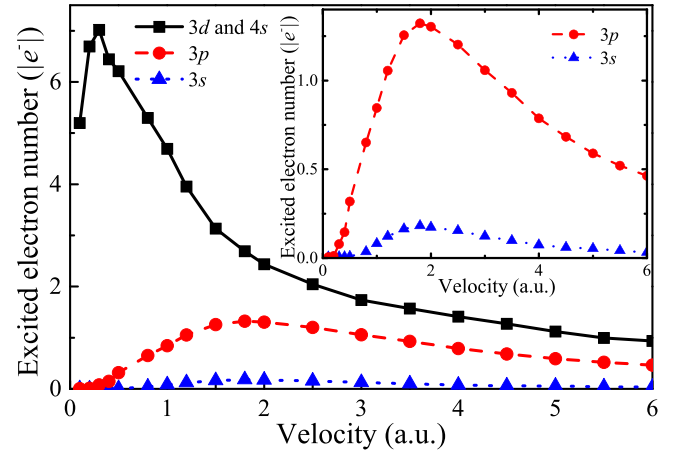


FIG. 4. Number of electrons excited from low-lying 3s, 3p bands and also from valence 3d and 4s bands for channeling proton in Ti12 as a function of velocity.

about 543 eV (higher than 2p binding energy 454 eV for Ti in this work) also takes place in the velocity regime above $v_{th} = 3.5$ a.u. Thus, we interpret that the underestimation of S_e for protons in Ti12 in the high-velocity regime mainly comes from neglecting lower-lying configurations.

Figure 5 presents the calculated S_e results for helium ions with velocity 0.1–6.0 a.u. along the channeling and the off-channeling geometries, and also the experimental data by Santry [60] and Sakamoto [63]. It can be seen that for helium ions channeled through Ti4, the underestimation of S_e begins at a very low velocity of about 0.2 a.u., and both the positions and amplitude of the stopping maximum are significantly lower than the experimental data. For helium ions in Ti12, the positions of the stopping maximum for channeling and off-channeling geometries posit at $v = 2.5$ a.u., coincident with the experimental data, while the amplitudes of both channeling and off-channeling S_e underestimate the experimental

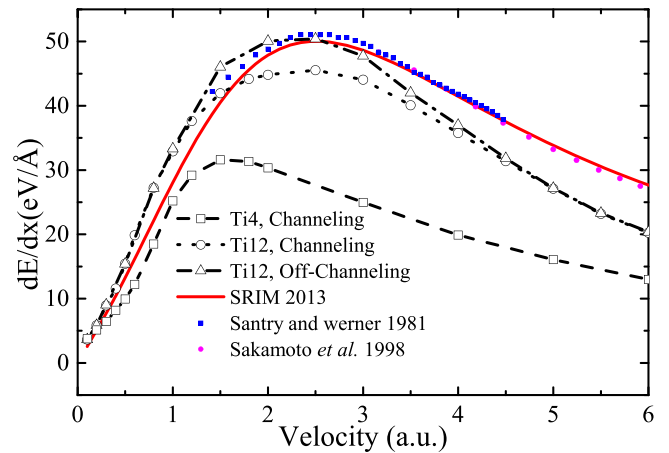


FIG. 5. Simulated electronic stopping power for channeling helium ion in Ti4 and Ti12 (black open squares and circles) and off-channeling protons in Ti12 (black open triangle) as a function of velocity, together with the SRIM-2013 predictions (red solid line) and also experimental data (solid symbols) by Santry [60] and Sakamoto [63].

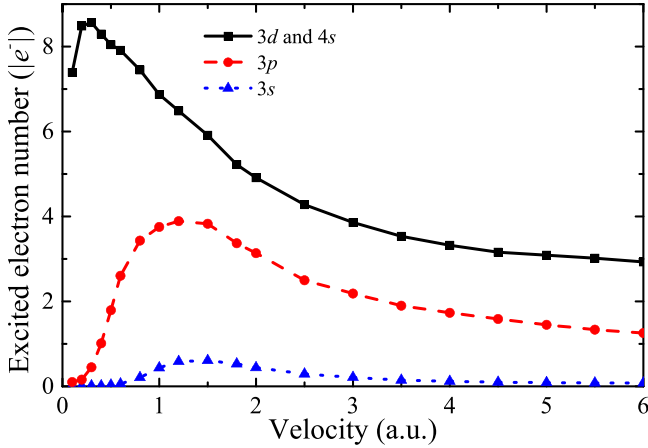


FIG. 6. Number of electrons excited from lower-lying $3s$, $3p$ bands and also from valence $3d$ and $4s$ bands for channeling helium ions in Ti12 as a function of velocity.

data for the velocity regime above the stopping maximum. For helium ion interactions with Ti12 under both channeling and off-channeling geometries, the underestimate in amplitude at $v = 5.0$ a.u. is about 18% compared with the experimental data.

We present in Fig. 6 the electronic excitation for helium ions in Ti12 under channeling condition. It is noted that for $3p$ band excitation, although there is a obvious change of curve slope at the threshold velocity 0.21 a.u., no hard threshold indeed exists due to slight excitation at lower velocities $v = 0.1$ and 0.2 a.u. Such results do not appear in lower-lying $3s$ band excitation. Considering that the depth of the $1s$ level of He is comparable with that of the $3p$ level of Ti, we interpret that it is the polarization effect of He ions that induced the diminish of hard threshold for $3p$ band excitation. Another finding is that, unlike the case for protons, whose positions of the maximum values of inner-shell excitation and electronic stopping are well matched, the trends of excited electrons in $3s$ and $3p$ bands saturate obviously earlier than the electronic stopping for helium ions. This result will be explained in the following part combining the charge state of the projectile.

To demonstrate in detail the general share of excitation on specific bands shown in Figs. 4 and 6, we show the proportions of electrons excited from specific bands for proton and helium ions in Fig. 7. For both proton and helium ions, proportions of inner $3s$ and $3p$ shell excitations increase with velocity and take a pronounced share in the high-velocity regime. It noted that the inner $3s$ and $3p$ shell excitations by helium ions take a considerable share even at low velocity ($v < 1$ a.u.), which accounts for the underestimation of S_e at the low-velocity regime for helium ions in Ti4 shown in Fig. 5, where $3s$ and $3p$ shell excitations are completely neglected.

Generally, for both proton and helium ions, the improvement in predicting electronic stopping brought by off-channeling geometry diminishes at the high-velocity regime, and the trend of S_e curves for channeling and off-channeling gets close to each other. Such results indicate that for projectiles with high-impact velocity, it is the explicit inclusion of more low-lying configuration that takes a major role in accurately determining the S_e , while tuning the impact

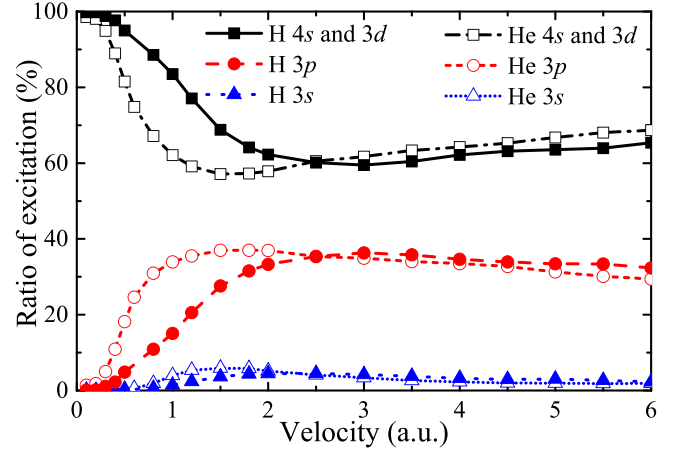


FIG. 7. Proportion of electrons excited from lower-lying $3s$ and $3p$ bands and also from valence $3d$ and $4s$ bands for channeling proton and helium ions in Ti12 as a function of velocity.

geometry makes a minor influence. We notice that, unlike the significant discrepancy in the position of the stopping maximum for projectiles in Ti4 and Ti12, there is no shift of position for the stopping maximum between the channeling and the off-channeling geometry for a projectile interacting with Ti12, indicating that the position of the stopping maximum is mainly dependent on the completeness of the electronic structure and insensitive to the impact parameter.

B. Charge state dependent electronic stopping

Furthermore, we calculate the charge states of projectiles when passing through the target using our recently proposed charge analysis method through the calculation of projected density of states (PDOS) on a specific orbital,

$$\rho_j(\varepsilon) = \sum_i \langle \varphi_i | j \rangle \langle j | \varphi_i \rangle \delta(\varepsilon - \varepsilon_i), \quad (5)$$

where ε_i is the eigenvalue of the eigenstate φ_i , and $\rho_j(\varepsilon)$ is the PDOS on the j orbital. Energy integrating of the $\rho_j(\varepsilon)$ below Fermi energy multiplied by the occupation number per state gives the number of bound electrons on the specific j orbital, whether it belongs to either the projectile or host atoms. A more detailed introduction of PDOS can be seen in Ref. [24].

We present in Fig. 8 the effective charge states (atomic number minus the bound electron number) of proton and helium ions. The electron number is obtained by averaging the bound electron on $1s$ orbitals over the same ion path as the calculation of stopping. It can be seen that for both proton and helium ions, the charge states increase monotonically with velocity until they reach fully deprived states at $v = 1.8$ and 3.5 a.u. for proton and helium ions, respectively. It is noted that the charge states do not decrease to zero at the very-low-velocity regime but begin to converge at $v = 0.3$ a.u. Similar results have been reported by Ojanperä [41] and Li [43] for lithium ion in graphene and diamond, respectively.

Now let us return to the mismatch of the positions for maximum values between inner-shell excitation and electronic stopping of helium in Ti12. As has been addressed in the former part, maximums of electronic stopping and the

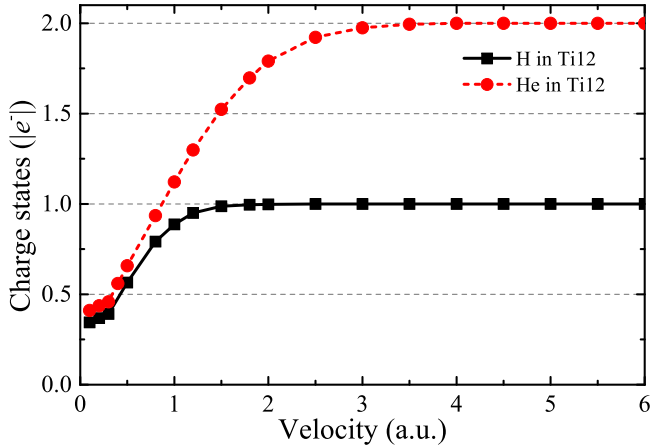


FIG. 8. Velocity-resolved effective charge states for channeling proton and helium ions in Ti12.

inner-shell excitation for protons are coincident, and they both occur at the velocity where the proton get fully deprived, while for helium ions, the inner-shell excitation maximum occurs at $v = 1.2$ a.u., and it gets fully deprived at $v = 3.5$ a.u. According to our previous work [43], the excitation energy (average energy dissipated in exciting per host electron) keeps increasing with velocity until it reaches the maximum around the velocity where it gets fully deprived. Thus, we interpret the fact that the stopping maximum occurs later than the inner-shell excitation maximum as a compromise of excited electron number and excitation energy.

We notice that, throughout the velocity regime considered, the effective charge of helium ions is higher than that of proton ions, and so is the amplitudes electronic stopping in Figs. 3 and 5. Such a result is in accordance with the corrected Lindhard linear response theory [16] that electronic stopping is in positive correlation with projectile charge state and depends quadratically on the effective charge state Z_{eff} of the projectile with velocity v . It is interesting to examine to what extent our calculated results match the linear response theory.

Figure 9 shows the ratios between proton and helium ions for calculated electronic stopping power and projectile

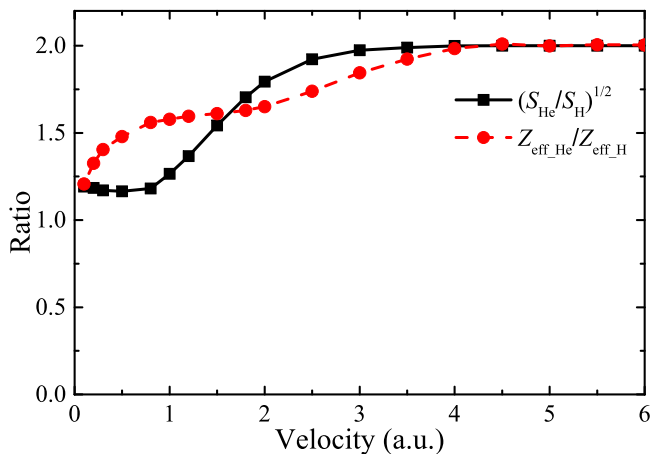


FIG. 9. Velocity-resolved ratios of electronic stopping and also effective charge states between channeling proton and helium ions in Ti12.

effective charge state. It can be seen that the two quantities are in good agreement at the high-velocity regime where the 1s electrons of both proton and helium ions are fully deprived. At low velocities, the divergence begins to appear, while the largest discrepancy is within 32%. As far as we know, other energy loss channels such as charge exchange [64–66] and chemical process [67] are also nonnegligible for a projectile that is only partially deprived. We interpret that the divergence in the low-velocity regime may come from other energy loss channels besides electron-hole creation that are not incorporated by linear response theory.

IV. CONCLUSIONS

We report a theoretical study from first principles on the nonadiabatic interaction of light ion with Ti in a wide range of velocities along the centroid channeling and also off-channeling geometries. It is found that the electronic stopping is significantly underestimated in the velocity regime around and above the stopping maximum with target inner-shell configurations frozen. The results are improved with core electrons explicitly included, indicating inner-shell excitations play a significant role in determining the amplitude of the stopping curve around and above the stopping maximum.

We also investigate the effect of impact geometry on electronic stopping. With the 3s and 3p band explicitly considered, quantitative agreement between the calculated electronic stopping power and the experimental data can be achieved nearly up to the stopping maximum under the centroid channeling condition, while for the velocity regime above the stopping maximum, the channeling stopping power significantly underestimates the experimental data. The result is improved by the off-channeling geometry, which makes possible the close encounter with the tightly bound electrons around the host nuclei. However, improvement brought by off-channeling geometry diminishes in the high-velocity regime, indicating that incorporating a more low-lying configuration plays a major role in determining the S_e , while tuning the impact geometry has a relative minor effect. We also find that, although there is divergence in the amplitude of electronic stopping between the channeling and off-channeling geometries, the positions of stopping maximums make no difference, suggesting that the position of the stopping maximum is not sensitive to the impact parameter.

Furthermore, we explore the correlation between electronic stopping and effective charge, and it is found that the electronic stopping is in positive relation to effective charge, and the stopping maximum occurs at around the velocity where projectiles get fully deprived. Our results about the relation between effective charge and electronic stopping are in qualitative agreement with the linear response theory.

ACKNOWLEDGMENTS

This work was supported by the National Natural Science Foundation of China under Grants No. 12135002 and No.12105205, and by the China Postdoctoral Science Foundation (Grants No. 2019M662693, No.2020T130486, and No. 2021M700003).

- [1] E. Rutherford, *Philos. Mag.* **21**, 669 (1911).
- [2] N. Bohr, *Philos. Mag.* **30**, 581 (1915).
- [3] H. Bethe, *Ann. Phys.* **397**, 325 (1930).
- [4] T. Diaz de la Rubia, H. M. Zbib, T. A. Khraishi, B. D. Wirth, M. Victoria, and M. J. Caturla, *Nature (London)* **406**, 871 (2000).
- [5] G. Ackland, *Science* **327**, 1587 (2010).
- [6] X. Wang and J. R. Key, *Science* **299**, 1725 (2003).
- [7] C. Bert, R. Engenhardt-Cabillic, and M. Durante, *Med. Phys.* **39**, 1716 (2012).
- [8] K. G. Reeves, Y. Yao, and Y. Kanai, *Phys. Rev. B* **94**, 041108(R) (2016).
- [9] R. Rando, A. Bangert, D. Bisello, A. Candelori, P. Giubilato, M. Hirayama, R. Johnson, H.-W. Sadrozinski, M. Sugizaki, J. Wyss, and M. Ziegler, *IEEE Trans. Nucl. Sci.* **51**, 1067 (2004).
- [10] H. Kraus, D. Simin, C. Kasper, Y. Suda, S. Kawabata, W. Kada, T. Honda, Y. Hijikata, T. Ohshima, V. Dyakonov *et al.*, *Nano Lett.* **17**, 2865 (2017).
- [11] Y. Zhang, I.-T. Bae, K. Sun, C. Wang, M. Ishimaru, Z. Zhu, W. Jiang, and W. J. Weber, *J. Appl. Phys.* **105**, 104901 (2009).
- [12] M. V. Moro, P. Bauer, and D. Primetzhofer, *Phys. Rev. A* **102**, 022808 (2020).
- [13] J. J. Thomson, *Philos. Mag.* **23**, 449 (1912).
- [14] C. G. Darwin, *Philos. Mag.* **23**, 901 (1912).
- [15] E. Fermi and E. Teller, *Phys. Rev.* **72**, 399 (1947).
- [16] J. Lindhard, *Phys. Lett.* **12**, 126 (1964).
- [17] C. P. Race, D. R. Mason, M. W. Finnis, W. M. C. Foulkes, A. P. Horsfield, and A. P. Sutton, *Rep. Prog. Phys.* **73**, 116501 (2010).
- [18] E. Runge and E. K. U. Gross, *Phys. Rev. Lett.* **52**, 997 (1984).
- [19] P. M. Echenique, R. M. Nieminen, J. C. Ashley, and R. H. Ritchie, *Phys. Rev. A* **33**, 897 (1986).
- [20] A. Arnau, M. Peñalba, P. M. Echenique, F. Flores, and R. H. Ritchie, *Phys. Rev. Lett.* **65**, 1024 (1990).
- [21] E. K. U. Gross and W. Kohn, *Phys. Rev. Lett.* **55**, 2850 (1985).
- [22] R. Ullah, F. Corsetti, D. Sánchez-Portal, and E. Artacho, *Phys. Rev. B* **91**, 125203 (2015).
- [23] M. Caro, A. Tamm, A. Correa, and A. Caro, *J. Nucl. Mater.* **507**, 258 (2018).
- [24] C.-K. Li, S. Liu, Q. Cao, F. Wang, X.-p. OuYang, and F.-S. Zhang, *Phys. Rev. A* **100**, 052707 (2019).
- [25] A. Lim, W. M. C. Foulkes, A. P. Horsfield, D. R. Mason, A. Schleife, E. W. Draeger, and A. A. Correa, *Phys. Rev. Lett.* **116**, 043201 (2016).
- [26] J. M. Pruneda, D. Sánchez-Portal, A. Arnau, J. I. Juaristi, and E. Artacho, *Phys. Rev. Lett.* **99**, 235501 (2007).
- [27] R. Ullah, E. Artacho, and A. A. Correa, *Phys. Rev. Lett.* **121**, 116401 (2018).
- [28] S. Datz, C. D. Moak, O. H. Crawford, H. F. Krause, P. F. Dittner, J. Gomez del Campo, J. A. Biggerstaff, P. D. Miller, P. Hvelplund, and H. Knudsen, *Phys. Rev. Lett.* **40**, 843 (1978).
- [29] V. V. Okorokov, *JETP Lett.* **2**, 111 (1965).
- [30] C.-K. Li, J.-m. Xue, X.-p. OuYang, and F.-S. Zhang, *Phys. Rev. A* **105**, 012819 (2022).
- [31] E. E. Quashie, B. C. Saha, and A. A. Correa, *Phys. Rev. B* **94**, 155403 (2016).
- [32] M. A. Zeb, J. Kohanoff, D. Sánchez-Portal, A. Arnau, J. I. Juaristi, and E. Artacho, *Phys. Rev. Lett.* **108**, 225504 (2012).
- [33] F. Mao, C. Zhang, J. Dai, and F.-S. Zhang, *Phys. Rev. A* **89**, 022707 (2014).
- [34] C.-K. Li, F. Wang, B. Liao, X.-P. OuYang, and F.-S. Zhang, *Phys. Rev. B* **96**, 094301 (2017).
- [35] C.-k. Li, F. Mao, F. Wang, Y.-l. Fu, X.-p. Ouyang, and F.-S. Zhang, *Phys. Rev. A* **95**, 052706 (2017).
- [36] A. A. Shukri, F. Bruneval, and L. Reining, *Phys. Rev. B* **93**, 035128 (2016).
- [37] D. C. Yost, Y. Yao, and Y. Kanai, *Phys. Rev. B* **96**, 115134 (2017).
- [38] Y. Yao, D. C. Yost, and Y. Kanai, *Phys. Rev. Lett.* **123**, 066401 (2019).
- [39] C.-W. Lee, J. A. Stewart, R. Dingreville, S. M. Foiles, and A. Schleife, *Phys. Rev. B* **102**, 024107 (2020).
- [40] A. Schleife, Y. Kanai, and A. A. Correa, *Phys. Rev. B* **91**, 014306 (2015).
- [41] A. Ojanperä, A. V. Krasheninnikov, and M. Puska, *Phys. Rev. B* **89**, 035120 (2014).
- [42] E. E. Quashie and A. A. Correa, *Phys. Rev. B* **98**, 235122 (2018).
- [43] C.-K. Li, J.-m. Xue, and F.-S. Zhang, *Phys. Rev. A* **106**, 022807 (2022).
- [44] X. Andrade, A. Castro, D. Zueco, J. L. Alonso, P. Echenique, F. Falceto, and A. Rubio, *J. Chem. Theory Comput.* **5**, 728 (2009).
- [45] A. A. Correa, J. Kohanoff, E. Artacho, D. Sánchez-Portal, and A. Caro, *Phys. Rev. Lett.* **108**, 213201 (2012).
- [46] J. P. Perdew and Y. Wang, *Phys. Rev. B* **45**, 13244 (1992).
- [47] N. T. Maitra, K. Burke, and C. Woodward, *Phys. Rev. Lett.* **89**, 023002 (2002).
- [48] V. U. Nazarov, J. M. Pitarke, Y. Takada, G. Vignale, and Y.-C. Chang, *Phys. Rev. B* **76**, 205103 (2007).
- [49] M. A. L. Marques, A. Castro, G. F. Bertsch, and A. Rubio, *Comput. Phys. Commun.* **151**, 60 (2003).
- [50] A. Castro, H. Appel, M. Oliveira, C. A. Rozzi, X. Andrade, F. Lorenzen, M. A. L. Marques, E. K. U. Gross, and A. Rubio, *Phys. Status Solidi B* **243**, 2465 (2006).
- [51] See Supplemental Material at <http://link.aps.org/supplemental/10.1103/PhysRevA.107.042813> for details regarding convergence of time step, grid spacing, and supercell size, and also comparison of results for electronic stopping along different direction.
- [52] C. Hartwigsen, S. Goedecker, and J. Hutter, *Phys. Rev. B* **58**, 3641 (1998).
- [53] L. Kleinman and D. M. Bylander, *Phys. Rev. Lett.* **48**, 1425 (1982).
- [54] I.-C. Yeh and M. L. Berkowitz, *J. Chem. Phys.* **111**, 3155 (1999).
- [55] B. A. Wells and A. L. Chaffee, *J. Chem. Theory Comput.* **11**, 3684 (2015).
- [56] A. Kononov and A. Schleife, *Nano Lett.* **21**, 4816 (2021).
- [57] Y. V. Gott and V. G. Tel'kovskii, *Radiotekh. Elektron.* **11**, 1956 (1962).
- [58] E. Arkhipov and Y. V. Gott, *Sov. Phys. JETP* **29**, 615 (1969).
- [59] J. Ormrod, *Nucl. Instrum. Methods* **95**, 49 (1971).
- [60] D. Santry and R. Werner, *Nucl. Instrum. Methods B* **188**, 211 (1981).
- [61] M. Brocklebank, S. N. Dedyulin, and L. V. Goncharova, *Eur. Phys. J. D* **70**, 248 (2016).

- [62] T. Otobe, M. Yamagiwa, J.-I. Iwata, K. Yabana, T. Nakatsukasa, and G. F. Bertsch, *Phys. Rev. B* **77**, 165104 (2008).
- [63] N. Sakamoto, H. Ogawa, N. Shiomi-Tsuda, M. Saitoh, U. Kitoba, and M. Ota, *Nucl. Instrum. Methods B* **135**, 107 (1998).
- [64] A. Arnau, M. Peñalba, P. M. Echenique, and F. Flores, *Nucl. Instrum. Methods B* **69**, 102 (1992).
- [65] D. Primetzhofer, *Phys. Rev. B* **86**, 094102 (2012).
- [66] R. A. Wilhelm, E. Gruber, R. Ritter, R. Heller, S. Facsko, and F. Aumayr, *Phys. Rev. Lett.* **112**, 153201 (2014).
- [67] C.-K. Li, F. Wang, C.-Z. Gao, B. Liao, X.-P. Ouyang, and F.-S. Zhang, *Nucl. Instrum. Methods B* **426**, 41 (2018).